

# Combustion synthesis of Ga<sub>2</sub>O<sub>3</sub> nanoparticles

V. Srihari · V. Sridharan · H. K. Sahu · G. Raghavan ·  
V. S. Sastry · C. S. Sundar

Received: 4 August 2008 / Accepted: 18 September 2008 / Published online: 11 December 2008  
© Springer Science+Business Media, LLC 2008

**Abstract** Nanophase of Ga<sub>2</sub>O<sub>3</sub> has potentially important applications in photocatalysis. We report the synthesis of nanophase of the metastable  $\gamma$ - and stable  $\beta$ -Ga<sub>2</sub>O<sub>3</sub> and demonstrate that it is possible to prepare a continuously varying mixture starting from the pure metastable  $\gamma$ - to the pure  $\beta$ -phase. This is achieved by employing a facile and reliable combustion route, using urea as a fuel. Typical grain sizes, as estimated from XRD studies, are about 3 nm. Given the importance of surface chemistry for potential applications, thermogravimetric coupled with mass spectrometry is used in conjunction with FTIR to elucidate the chemistry of the adsorbed surface layer. Studies on the  $\gamma$ -Ga<sub>2</sub>O<sub>3</sub> phase indicate the occurrence of weight loss of 8.1% in multiple steps. Evolved gas analysis and FTIR studies show presence of physisorbed H<sub>2</sub>O molecules and chemisorbed  $-(OH)$  ions bonded to active surface states and accounts predominantly for the observed weight loss.

## Introduction

The remarkable photocatalytic properties of anatase TiO<sub>2</sub> have been widely studied and documented in the literature for decades now [1 and references therein]. With the advent of novel techniques for nanophase synthesis, it has

been realized that the nanophase counterpart of bulk TiO<sub>2</sub> is more efficient for photocatalysis. It has also been shown that a 30/70% mixture of the rutile/anatase phases is optimal rather than the pure anatase phase for technological purposes. The potential applications of this material range from photodegradation of hazardous waste, bio-corrosion to more exotic ones such as self-cleaning apparel. Through our recent work, it has been realized that nanoparticles of  $\beta$ -Ga<sub>2</sub>O<sub>3</sub> is highly effective in the photodegradation of certain hazardous chemicals [2]. Given the experience with TiO<sub>2</sub>, this naturally raises the question whether a mixed phase of Ga<sub>2</sub>O<sub>3</sub>, specifically  $\beta$ - and  $\gamma$ -Ga<sub>2</sub>O<sub>3</sub> mixture, present in a certain ratio would be optimal. While  $\beta$ -Ga<sub>2</sub>O<sub>3</sub> is the stable phase,  $\gamma$ -Ga<sub>2</sub>O<sub>3</sub> is metastable and undergoes a structural transformation to  $\beta$ -phase above 600 °C [3]. Being a metastable phase,  $\gamma$ -phase could not be prepared through conventional routes and sparse references are available on it [4–6]. Investigations indicate that metastable phases of materials could have greater stability in the nanophase form relative to their bulk counterparts. With this as background, we investigated the possibility of using the urea combustion route to synthesize nanophase of  $\gamma$ - and  $\beta$ -Ga<sub>2</sub>O<sub>3</sub>. In the present work, we demonstrate that by controlling the quantity of fuel (urea), it is possible to prepare not only the elusive  $\gamma$ -phase but continuously vary the composition from pure  $\gamma$ - to pure  $\beta$ -Ga<sub>2</sub>O<sub>3</sub>. Particle sizes obtained through this route are of typically a few nanometres.

The surface chemistry of the material under investigation is found to play a pivotal part in the photocatalytic degradation of certain chemicals. Hence, studies on surface chemistry are germane and important. With this in mind, we have carried our mass-spectrometry coupled thermogravimetry studies on the as-combusted product. The information obtained thereof is complemented by FTIR

---

V. Srihari · V. Sridharan (✉) · H. K. Sahu · G. Raghavan ·  
V. S. Sastry · C. S. Sundar  
Materials Science Division, Indira Gandhi Centre for Atomic  
Research, Kalpakkam 603 102, India  
e-mail: varadu@igcar.gov.in; sridh61@hotmail.com

V. Srihari  
e-mail: vsrihari\_kjgm@yahoo.co.in

which is used to elucidate the surface chemistry of our specimens.

### Experimental details

Gallium nitrate was prepared by dissolving pure gallium metal (99.99+) in concentrated  $\text{HNO}_3$  (GR grade) heated to 60 °C to obtain a clear solution. Distilled water was added to this solution, and maintained at 80 °C overnight to remove excess  $\text{HNO}_3$ . The solution was allowed to cool in a vacuum desiccator to yield a pale milky-white  $\text{Ga}(\text{NO}_3)_3 \cdot x\text{H}_2\text{O}$  solid. Due to its deliquescent nature,  $\text{Ga}(\text{NO}_3)_3 \cdot x\text{H}_2\text{O}$  was stored under dynamic vacuum. Following the prescription of Jain et al. [7], the amount of urea required for combustion was calculated from the stoichiometric ratio

$$\Phi_c = \frac{\text{No. of oxidising valency}}{(-1) \text{ No. of reducing valency}} \quad (1)$$

which for  $\text{Ga}_2\text{O}_3$  is:

$$\Phi_c = \frac{3(\text{Ga}) + 0(\text{N}) + 3(-6(\text{O}))}{(-1)[4(\text{C}) + 4(1(\text{H})) + 2(0(\text{N})) + (-2)(\text{O})]} = \frac{-15}{-6} = 2.5 \quad (2)$$

Corresponding to  $\Phi_c = 2.5$ , 1.13 g of  $\text{Ga}(\text{NO}_3)_3 \cdot x\text{H}_2\text{O}$  was dissolved in distilled water along with 0.66 g of urea (99.5%) corresponding to a weight ratio (WR) of 1.7. One of the crucial factors influencing reaction kinetics during combustion is the fuel content. With a view to examine the role of fuel content on the formation of the final phase, we have prepared a series of samples, varying only the urea content as a control parameter; going from “sub-stoichiometric”, “stoichiometric” to “super-stoichiometric” ratios of the fuel. The quotes are essential to bear in mind that the amount of water in the gallium nitrate is undetermined in the weighing process. Accordingly, urea content, varied as 0.35, 0.54, 0.94 and 1.13, was mixed with 1.13 g of gallium nitrate corresponding to WR = 3.2, 2, 1.2 and 1. The solutions were heated at 80 °C under constant stirring till a white paste results. The pastes were placed in separate BOROSIL beakers and individually combusted by loading into a furnace, preheated to 500 °C. Combustion lasting for a second or so, results in a highly, spindly network structure much like cotton candy. As-combusted products (ACP) corresponding to WR of 3.2, 2, 1.5, 1.2 and 1 are denoted as samples *a*, *b*, *c*, *d* and *e* respectively.

Room-temperature powder X-ray diffraction (XRD) patterns were recorded using a STOE diffractometer in  $2\theta$  range 12–70° in steps of 0.05°. The average grain size  $\langle R \rangle$  was estimated using the Scherrer equation [8]. The

observed widths of the diffraction peaks were corrected for the instrumental broadening as

$$\Gamma^2 = \Gamma_{\text{Obs}}^2 - \Gamma_{\text{Inst}}^2 \quad (3)$$

where  $\Gamma_{\text{Obs}}$  is the observed width of a profile fitted to a Gaussian and the  $\Gamma_{\text{Inst}}$  is the instrumental contribution to broadening which was predetermined from the XRD pattern of NIST Si polycrystalline powder. DTA measurement was carried out on Mettler Toledo STAR<sup>c</sup> system. A SETARAM-make Thermogravimetric (TGA) analyzer was used for weight loss studies and a home-built mass spectrometer attached to it was used for evolved gas analysis. Both DTA and TGA measurements were carried out at a heating rate of 20 °C/min using argon as a purge gas and calcined alumina as a reference material. FTIR absorption spectra of the specimens in KBr matrix were recorded using a Bomem DA8 spectrometer operating with a resolution of 4  $\text{cm}^{-1}$ .

### Results and discussions:

The XRD pattern of sample *a–e* is shown in Fig. 1, along with that of bulk polycrystalline  $\beta\text{-Ga}_2\text{O}_3$  (99.999%), obtained from Alfa-Aesar, UK. The XRD pattern of sample *a* exhibits broadened reflections corresponding to  $\beta\text{-Ga}_2\text{O}_3$ . With the decreasing urea content (samples *a–e*), broad features at  $2\theta \approx 36^\circ$  and  $60^\circ$  develop at the expense of the  $\beta\text{-Ga}_2\text{O}_3$  reflections and for the sample *e*, only the broad features are present. The DTA thermogram, in the temperature range of 35–900 °C, for sample *e* is shown in Fig. 2. It exhibits a strong and asymmetric endotherm peaked at  $T_p = 127^\circ\text{C}$  and a relatively sharp exotherm at

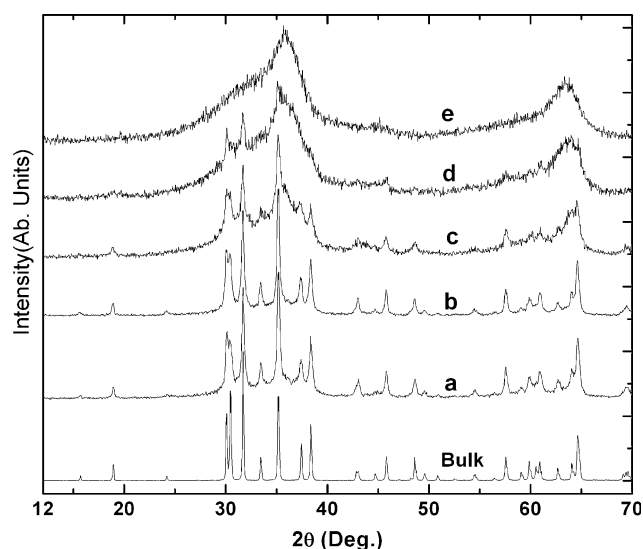


**Fig. 1** Room-temperature powder X-ray diffraction pattern of samples *a–e* along with that of the bulk polycrystalline sample

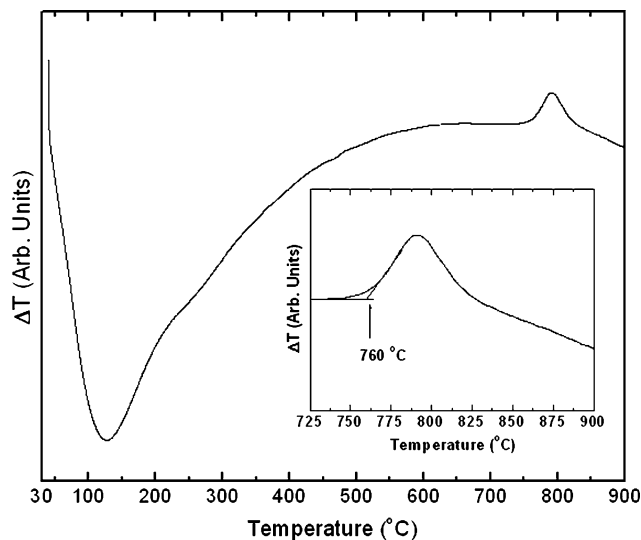


**Fig. 2** Differential thermal analyzer thermogram of sample *e*. Heating rate: 20 °C/min; Purge gas: Argon. Inset shows exothermic peak with an onset temperature of 760 °C

$T_p = 791$  °C with an onset temperature of 760 °C. The endotherm stretches to  $\sim 603$  °C and exhibits high-temperature substructures reminiscent of multiple endotherms. Figure 3 shows the TGA thermogram of sample *e*, along with calculated derivative-TGA (DTGA) curve. Weight loss starts from just above room temperature and extends to  $\sim 800$  °C with distinct weight loss steps which are exemplified in the DTGA curve. Total weight loss is estimated to be 8.1%. In Fig. 4, the FTIR spectra of samples *a–e* in the range of 1300–4000  $\text{cm}^{-1}$  are compared. All the samples exhibit a relatively weak absorption band at 1350  $\text{cm}^{-1}$ , a sharp absorption band at 1600  $\text{cm}^{-1}$  and a

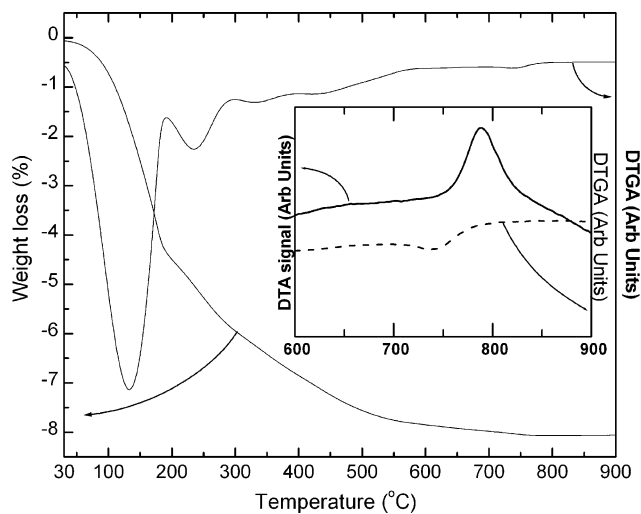


**Fig. 3** Thermogravimetric analyzer thermogram of sample *e* along with its computed derivative (DTGA). Heating rate: 20 °C/min; Purge gas: Argon. Inset compares the DTA and DTGA thermogram in the temperature interval of 600–900 °C

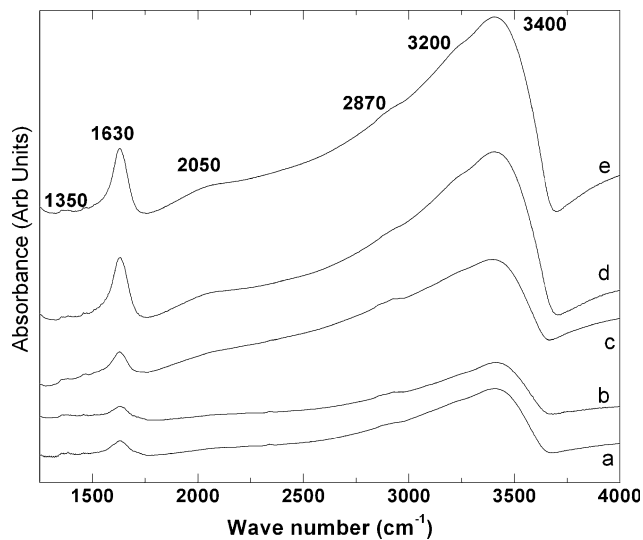


**Fig. 4** FTIR spectrum of samples *a–e* in the range of 1300–4000  $\text{cm}^{-1}$

broad and dominant absorption band in the range of 2000–3600  $\text{cm}^{-1}$  with overriding weak peak structures.

On comparing with the reflections (Fig. 1) of polycrystalline  $\beta\text{-Ga}_2\text{O}_3$ , it is clearly seen that sample *a* is a single-phase, stable  $\beta\text{-Ga}_2\text{O}_3$ . Observed broadening of the reflections originate from particle size effects. From the width of the isolated (002) reflection of the  $\beta\text{-Ga}_2\text{O}_3$  at  $2\theta \approx 18.9^\circ$ , the average grain size is determined to be 31 nm. While  $\langle R \rangle$  was estimated to be 30 and 5 nm respectively for the samples *b* and *c*, same could not be estimated for sample *d* for want of well-defined (002) reflection. The significantly broadened profiles of sample *e*, throw open an entirely new possibility that it may either correspond to the  $\beta\text{-Ga}_2\text{O}_3$  phase with a still lower grain size ( $<5$  nm), or to the emergence of an entirely new phase. The XRD pattern of the sample *e* exhibits broad profiles with assignable peaks at  $2\theta$  at  $\approx 31, 31.5, 55.5, 59.1$  and  $63.5^\circ$ . These peaks closely match with that of earlier works which were ascribed to a metastable  $\gamma\text{-Ga}_2\text{O}_3$  [3, 4]. If sample *e* is the metastable  $\gamma\text{-Ga}_2\text{O}_3$ , it goes to reason that it would transform to the stable  $\beta$ -phase under heat treatment. Indeed, the DTA thermogram (Fig. 2) of sample *e* exhibits an exotherm with an onset temperature of 760 °C. Further, XRD pattern (not shown) of the post-DTA-run sample confirms the occurrence of a transformation to the  $\beta\text{-Ga}_2\text{O}_3$ . Both the results indicate that sample *e* is the metastable  $\gamma\text{-Ga}_2\text{O}_3$ . As the reflections of  $\gamma\text{-Ga}_2\text{O}_3$  rather closely spaced, the XRD pattern of sample *e* is not amenable for grain size analysis as in the case of other samples. Hence, XRD pattern for the  $\gamma\text{-Ga}_2\text{O}_3$  was simulated using reported peak positions and relative intensities [3, 9] and assuming the Gaussian profile. In doing so, the width of the peaks was constrained to follow the Scherrer equation [8].

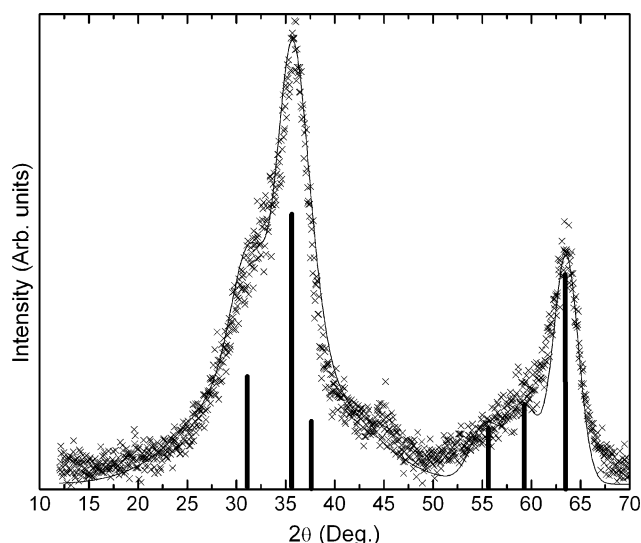


**Fig. 5** Simulated (solid line) XRD pattern for  $\gamma$ -Ga<sub>2</sub>O<sub>3</sub> corresponding to  $\langle R \rangle = 3$  nm is compared with that of the observed (x). Vertical lines indicate the position of the Bragg peaks and their relative intensities as per [9]. See the text for details

It is seen that such a simulated XRD pattern, corresponding to  $\langle R \rangle = 3$  nm, compares well with that of sample *e* (Fig. 5). This indicates that sample *e* is a nanophase of  $\gamma$ -Ga<sub>2</sub>O<sub>3</sub> with  $\langle R \rangle = 3$  nm. Thus, it is seen, from the analysis of the XRD patterns, that while samples *a* (combusted with super-stoichiometric urea) and *e* (combusted with sub-stoichiometric urea) are the stable  $\beta$ - and metastable  $\gamma$ -Ga<sub>2</sub>O<sub>3</sub> nanophase respectively, samples *b*, *c* and *d* are a mixture of  $\gamma$ - and  $\beta$ -phases. In other words, the present work demonstrates that one can employ the combustion method to reliably synthesize nanophase of  $\beta$ - and  $\gamma$ -Ga<sub>2</sub>O<sub>3</sub> and more importantly a mixture of them by controlling the fuel content alone. The possibility of continuously varying the mixture of phases is highly attractive, especially for use of this material in the photocatalytic reaction as has been shown in the case of TiO<sub>2</sub> [1].

Having established the robustness of the synthesis procedure, we now focus on the presence of adsorbed species on the active surface states of the nanophased specimens. As indicated earlier, these studies are of importance to end-use in technological applications. The nanophase of  $\gamma$ -Ga<sub>2</sub>O<sub>3</sub> undergoes a weight loss of 8.1%, less than reported for nanophase of anatase-TiO<sub>2</sub> [10]. Similarity between the endothermic peak of DTA and the DTGA imply that the endotherm events are to be associated with weight loss events. In the inset of Fig. 3, the DTGA and DTA thermograms in the temperature interval of 600–900 °C are compared. It is clearly seen that the weight loss event is well separated from the exothermic event. From evolved gas analysis (not shown) it is seen that evolution of H<sub>2</sub>O and  $-(OH)$  dominate the observed

weight losses, with maximum of evolution closely matching with DTA thermogram. Though evolution of CO<sub>2</sub> and N<sub>2</sub> are also observed, their partial pressures are much less compared to that of H<sub>2</sub>O and  $-(OH)$  species and may be neglected.

While the weak absorption band (Fig. 4) at 1600 cm<sup>-1</sup> is associated with the vibration mode for O–H–O bonds of the physisorbed water [10], the much weaker absorption at 1350 cm<sup>-1</sup> is ascribed to CO<sub>3</sub><sup>2-</sup> and HCO<sub>2</sub><sup>2-</sup> ions [11]. The dominant absorption assignable to  $-(OH)$  stretching mode exhibits structures peaking at  $\approx 2050$ , 2870, 3200 and 3400 cm<sup>-1</sup>. The absorption band located at 3400 cm<sup>-1</sup> is ascribed to hydroxyl group of Ga–OH at the active sites at the surface with which physisorbed water molecules are bound by weak hydrogen bonds with (OH)– of Ga<sub>2</sub>O<sub>3</sub> surfaces [12]. It is proposed that other  $-(OH)$  absorption bands arise from similar chemisorbed states but with weaker bonding with surface states. As such, the nature of the active surface states is expected to be independent of underlying crystallographic structure ( $\gamma$ - or  $\beta$ -Ga<sub>2</sub>O<sub>3</sub>), and therefore, the  $-(OH)$  absorption band appears similar in its structure across the samples *a–e*. Observation of  $-(OH)$  absorption band with structures for the anatase-TiO<sub>2</sub> nanophase [10] lends support to our inference. Decrease of physisorbed and chemisorbed band with increase of fuel content can be understood in terms of a dramatic decrease of number of active surface states with increase in the  $\langle R \rangle$  from  $\sim 3$  (sample *e*) to  $\sim 31$  nm (sample *a*). Hence, the weight loss at about 120 °C is ascribed to physisorbed H<sub>2</sub>O molecules and successive weight loss steps to evolution of chemisorbed  $-(OH)$  bound to active surface states with different bonding strengths. To ascertain if the presence of CO<sub>3</sub><sup>2-</sup> ions and H<sub>2</sub>O and  $-(OH)$  ions is the result of incomplete combustion and use of aqueous media for combustion synthesis respectively, sample *e* was heated for 30 min, to minimize the grain growth, at 800 °C at which temperature the sample had completed its weight loss of 8.1% even under dynamic mode (Fig. 2). Sample was then quickly cooled to room temperature and exposed to ambient for 30 min before recording FTIR spectrum. Resulting FTIR spectrum (not shown) is essentially same as that of Fig. 4e with negligible changes in the relative intensity. On the other hand, the FTIR spectrum (not shown) of the sample heat treated at 1200 °C, corresponding to bulk polycrystalline, did not show absorbance in the range of 1300–4000 cm<sup>-1</sup>. Hence, the FTIR studies on as-combusted nanophase samples and on heat-treated samples confirm that adsorbed species are neither due to incomplete combustion nor due to the use of aqueous media but to presence of highly active surface states of the products to which gaseous species in the ambient get readily attached.

## Conclusions

Nanoparticles of Ga<sub>2</sub>O<sub>3</sub> were synthesized through combustion route using urea as fuel. Both the stable  $\beta$ -phase and the metastable  $\gamma$ -phase of Ga<sub>2</sub>O<sub>3</sub> in nanometric sizes were stabilized by varying the fuel to material ratio. While lower fuel content stabilizes the metastable  $\gamma$ -phase, higher fuel content stabilizes stable  $\beta$ -phase. Average grain size of as-combusted  $\gamma$ - and  $\beta$ -phase, as determined from the width of the X-ray diffraction peaks, were typically in the range of 4–30 nm. Active surface states present in the as-combusted products react with ambient leading to physisorbed H<sub>2</sub>O molecules and  $-(OH)$  and CO<sub>3</sub><sup>2-</sup> ions.

**Acknowledgement** The authors thank Premila for recording FTIR spectrum and for useful discussion on the FTIR spectrum.

## References

1. Diebold U (2003) Surf Sci Rep 48:53
2. Seshadri H, Sridharan V, Sasidhar P, Sinha PK, Sastry VS, Sundar CS (2008) In: International conference on nano and microelectronics, 3–5 January 2008, Pondicherry Engineering College, Pondicherry, India
3. Roy R, Hill VG, Osborn EF (1952) J Am Chem Soc 74:719
4. Delgado MR, Areal CO (2003) Mater Lett 57:2292
5. Areán CO, Bellan AL, Mentruit MP, Delgado MR, Palomino GT (2000) Micropor Mesopor Mater 40:35
6. Ristic M, Popovi TS, Music S (2005) Mater Lett 59:1227
7. Jain SR, Adiga KC, Pai Verneker VR (1981) Combust Flame 40:71
8. Cullity BD (1977) Elements of X-ray diffraction. Addison-Wiley Publishing Company, Inc, Reading
9. ICDD Card No. 060529
10. Li G, Li L, Boerio-Goates J, Woodfield BF (2005) J Am Chem Soc 127:8659
11. Bezrodna T, Puchkovska G, Shimanovska V, Chashechnikova I, Khalyavka T, Baran J (2003) Appl Surf Sci 214:222
12. Bezrodna T, Puchkovska G, Shymanovska V, Baran J, Ratajczak H (2004) J Mol Struct 700:175